Empirical Equation of the Mach Number as a Function of the Stagnation Pressure Ratio for a Quasi-One-Dimensional Compressible Flow

San Luis Tolentino
MSc. Mech. Ing.
National Experimental Polytechnic University "AJS" Vice-Rectorate (UNEXPO)
Puerto Ordaz
Bolívar
Venezuela
Research collaborator
Group of Mathematical Modeling and Numerical Simulation (GMMNS)
National University of Engineering (UNI)
Lima
Perú

In the present work for a quasi-one-dimensional isentropic compressible flow model, an empirical equation of the Mach number is constructed as a function of the stagnation pressure ratio for an analytical equation that algebraic procedures cannot invert. The Excel 2019 Solver tool was applied to calibrate the coefficients and exponents of the empirical equation during its construction for the Mach number range from 1 to 10 and 1 to 5. A specific heat ratio from 1.1 to 1.67 and the generalized reduced gradient iterative method were used to minimize the sum of squared error, which was set as the objective function. The results show that for Mach 1 to 10, an error of less than 0.063% is obtained, and for Mach 1 to 5, an error of less than 0.00988% is obtained. It is concluded that the empirical equation obtained is a mathematical model that reproduces the trajectories of the inverted curves of the analytical equation studied.

Keywords: *objective function, generalized reduced gradient, empirical equation, Mach number, quasi-one-dimensional flow, stagnation pressure.*

1. INTRODUCTION

The numerical characteristics for compressible flow in convergent-divergent nozzles vary mainly in the flow direction. They can be considered given by its appro–ximation as quasi-one-dimensional isentropic flow. Isentropic flow assumes a steady state, a perfect gas, and a non-viscous fluid [1-3].

In viscous flows, vortex generation, boundary layer detachment, flow separation, and recirculation are present [4-6]; the sensitivity of the Mach disk shape to radial pressure gradients [7]. As well as the flow sepa–ration modes present characteristics defined in truncated ideal contour (TIC), thrust optimized contour (TOC), thrust optimized parabolic (TOP), conical nozzle types [8-10], planar nozzles [11, 12] and diffusers [13, 14].

It should be noted that for ideal flows, quasi-one-dimensional models have applications in wind tunnels, nozzles, and diffusers, among others [2-4]. Reference is made to some wind tunnel tests, such as the experi–mental study on the influence of the length of the spike on the aerodynamic characteristics of blunt bodies for various angles of attack and Mach and Reynolds numbers [15]. Study of experimental tests on the calibration of a wind tunnel, where a calibration model is used that represents a generic configuration of a winged missile [16.17] presents comparative results for the standard AGARD-B model in the transonic speed range tested in six wind tunnels. That model is a simple configuration of a high-speed delta-winged air–plane. As well as in [18], they also report the experimental evaluation of eight SZ-1500 series airfoils for low Reynolds numbers tested in a wind tunnel.

A shock wave is an intense pressure wave that travels faster than the speed of sound. The normal shock wave occurs in the diverging section for a quasi-one-dimensional flow and under the nozzle's inlet and outlet pressure conditions. In the region where the shock occurs, the process is irreversible, and the entropy increases; in that region of the shock, the process is not considered an isentropic process, and whose shock thickness is extremely thin on the order of 10^{-5} cm according to Anderson [2].

The analysis for a steady flow without heat transfer, for a control volume of a shock wave, considers the principles of conservation of mass, energy, momentum, and state.Furthermore, by intercepting the Fanno and Rayleigh curves, the limits of the thermodynamic parameters are defined before and after the shock [1, 19, 20]. The first analyses of these relations are due to Rankine (1870) and Hugoniot (1887), known as Rankine-Hugoniot relations.

The dominant parameter for a compressible flow is the Mach number M, and it is classified as subsonic for $0.3 \leq M \leq 0.8$, transonic $0.8 \leq M \leq 1.2$, supersonic $1.2 \leq M \leq 5$, hypersonic $M > 5$, and sonic $M = 1$ [2].

1.1 Normal shock wave in a nozzle

A simple scheme of a convergent-divergent nozzle is shown in Fig. 1a; in the position of local area ratio A_x/A^* and stagnation pressure ratio P_{oy}/P_{ox}, a normal shock wave is located, where A_x is the cross-sectional area in the shock position and A^* the throat area. The geometric parameter of the convergent is the half angle β, and of the divergent is the half angle α. At the inlet of the nozzle is the stagnation pressure P_0 (total pressure), whose pressure

Received: June 2022, Accepted: March 2023
Correspondence to: San Luis Tolentino, Group of Mathematical Modeling and Numerical Simulation, National University of Engineering (UNI), Lima, Perú
E-mail: sanluist@gmail.com
doi: 10.5937/fme2302149T

has the same magnitude in the combustion chamber, in the convergent, and the divergent until the shock position at x, where $P_o = P_{ox}$. After the shock, at position y, there is the stagnation pressure P_{oy}, whose magnitude is the same up to the nozzle outlet. The exhaust area A_e, the static pressure P_e and the Mach number M_e at subsonic velocity are found at the nozzle exit [1,3].

The trajectory of the Mach number curve is shown in Fig. 1b. The divergent shows the behavior of the Mach number pattern before and after the shock, where the flow goes from supersonic velocity to subsonic velocity; for these conditions, the flow is classified as over-expanded flow [2,3].

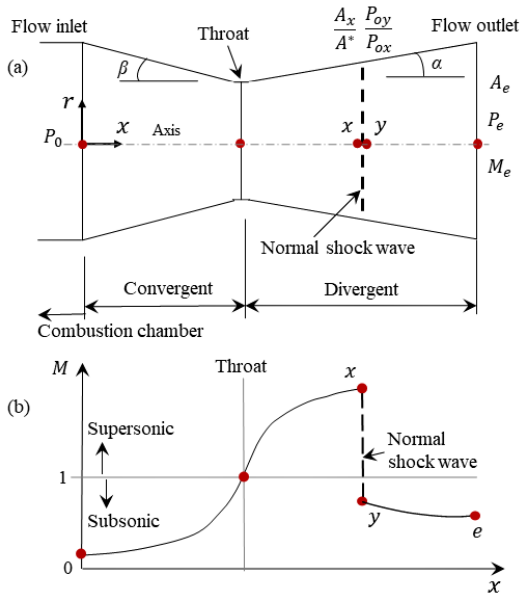

Figure 1. A simple scheme of a convergent-divergent nozzle. (a) The divergent section refers to the position of a normal shock wave. (b) Flow rate pattern in terms of the Mach number. Adapted from Anderson [2]

In the gas dynamics for compressible flow, the value of k is variable and is a thermodynamic parameter of the gas. It is known as the specific heat ratio; this parameter is a positive value, and it is in the range of $1 < k \leq 1.67$. For air, the value is $k = 1.4$; for other gases, such as those generated by the combustion of solid, liquid, and hybrid fuels used in rocket engines, the value of k is less than 1.4 [3].

For an over-expanded isentropic flow, the calculations begin with the pressure ratio P_e/P_0, whose value is previously determined under the condition that the shock is present in the divergent at an arbitrary position A_x/A^* (Figure 1a), being P_e less than atmospheric pressure. In addition, we have the area ratio A_e/A^* for the design condition. The use of analytical equations is mentioned below.

At the nozzle exit, the subsonic Mach number M_e is determined by equation (1) [1]:

$$M_e = \left[\left[\frac{\left(\frac{2}{k-1}\right)\left(\frac{2}{k+1}\right)^{\left(\frac{k+1}{k-1}\right)}}{\left(\frac{A_e P_e}{A^* P_0}\right)} + \frac{1}{(k-1)^2} \right]^{0.5} - \frac{1}{(k-1)} \right]^{0.5} \quad (1)$$

The ratio of stagnation pressures P_{oy}/P_{ox} is determined by equation (2) [1], which is a function of M_e:

$$\frac{P_{0y}}{P_{0x}} = \frac{P_e}{P_o}\left[1 + \left(\frac{k-1}{2}\right)M_e^2\right]^{\left(\frac{k}{k-1}\right)} \quad (2)$$

P_{0y}/P_{0x} is substituted in equation (3) [1], and by iterative methods, the supersonic Mach number M_x is determined at the position of the shock, at reference x:

$$\frac{P_{oy}}{P_{ox}} = \frac{\left[\frac{M_x^2}{\frac{2}{(k+1)} + \left(\frac{k-1}{k+1}\right)M_x^2}\right]^{\left(\frac{k}{k-1}\right)}}{\left[\left(\frac{2k}{k+1}\right)M_x^2 - \left(\frac{k-1}{k+1}\right)\right]^{\left(\frac{1}{k-1}\right)}} \quad (3)$$

With equation (4) [1] is calculated A_x/A^* at the position of the shock, for $M = M_x$:

$$\frac{A}{A^*} = \frac{1}{M}\left[\left(\frac{2}{k+1}\right) + \left(\frac{k-1}{k+1}\right)M^2\right]^{\left(\frac{k+1}{2k-2}\right)} \quad (4)$$

The subsonic Mach number M_y at the shock position, at the y reference, is calculated with equation (5) [1]:

$$M_y = \left[\frac{M_x^2 + \frac{2}{k-1}}{\frac{2k}{k-1}M_x^2 - 1}\right]^{0.5} \quad (5)$$

The static pressure ratio P_y/P_x at the shock position is determined with equation (6) [1], which is useful to determine the minimum pressure drop P_x at the supersonic speed position M_x. Where P_y is the pressure reached when the flow slows down after the shock at position M_y:

$$\frac{P_y}{P_x} = \frac{2k}{k+1}M_x^2 - \frac{k-1}{k+1} \quad (6)$$

The calculations for equations (4), (5), and (6) are stopped since M_x is determined by iterative methods from equation (3). Equation (4) is known as the Stodola equation. Calculating the Mach number as a function of the area ratio is useful. To obtain the solution, iterative methods are applied; this equation has two solutions, one for subsonic flow and one for supersonic flow.

The analytical equations (3) and (4) cannot be inverted by algebraic procedures for solving the Mach number and are nonlinear problems. Therefore, some known method or other mechanisms must be applied to obtain empirical equations that yield approximate solutions for these two analytical equations.

As a scientific methodology, heuristics is a set of methods and techniques that allow finding a satisfactory solution to a problem, and Polya [21] explains how to approach it. In engineering sciences, empirical equations are very common to obtain approximate solutions to certain problems, such as fluid mechanics, heat transfer,

and deformations of solid materials, among others. The complexity of constructing empirical equations lies in the methods and tools used to obtain them.

Lagrange's inversion theorem is reported in the literature, which allows inverting analytic equations by means of the Taylor series expansion of the inverse function of an analytic function. This theorem was generalized by Bürmann [22].

The Stodola equation (4) was approached by Abu-Irshaid [23], who applied Bürmann's theorem to obtain a mathematical expression for an approximate solution; for values close to Mach 1, the series required more terms to reduce the error. Authors such as Majdalani and Maicke [24,25] also applied Bürmann's theorem to the Stodola equation (4) and obtained results similar to those reported in [23] for values close to Mach 1.

For further studies of compressible flow, Ferrari [26] applied the Abel equation to obtain new analytical solu–tions for the steady-state one-dimensional viscous adia–batic flow of an ideal gas through a conical nozzle or diffuser.

On the other hand, for the case of incompressible flow, such as the case of obtaining the explicit solution of the nonlinear Colebrook equation, different resear–chers applied other methods, such as the application of infinite recursion [27] and the Wright-ω function [28].

From the above, the application of different methods to obtain approximate solutions to implicit equations in fluid mechanics is observed. In that sense, since the solution of the analytical equation (3) is of great impor–tance to obtain direct calculations of the Mach number M_x for supersonic flow at the shock position at A_x/A^*, it has been proposed to obtain the solution by applying a method different from the mentioned methods.

In the present work, the objective is to construct an empirical equation for the Mach number as a function of the stagnation pressure ratio for a quasi-one-dimensi–onal compressible flow, which satisfies as an approxi–mate solution the inverse of the analytical equation (3).

The methodology presents the applied steps that allowed for constructing the empirical equation. The coefficients and exponents during construction of the empirical equation are calibrated with the *Solver* iterative simulation analysis tool in Excel 2019. The results of four case studies and the conclusions of the analysis are presented.

2. METHODOLOGY

2.1 Squared error conditioning based on fixed data and variable data

First, in general, the squared error e^2 is conditioned so that it can be applied to a standard data set that is considered fixed data for the position (x_i,y_i), and to a data set that is considered variable data for the position (x_i, y'_i), but only y'_i varies since x_i is the same parameter for both fixed and variable data. Fig. 2 illustrates the positions of the fixed data starting at position (x_1,y_1) and ending at position (x_n,y_n), and of the variable data starting at position (x_1,y_1) and ending at position (x_i, y'_n).

The squared error is expressed as:

$$e^2 = \left(y_i - y'_i\right)^2 \tag{7}$$

It should be noted that fixed data is associated with experiments, implicit analytic functions, and inverted data from analytic equations. The variable data are associated with an empirical equation under construction $y'_i = h(x_i)$, composed of trigonometric, polynomial, logarithmic, and exponential functions. The empirical equation's purpose is to be well structured to model the curve's path on the fixed data faithfully.

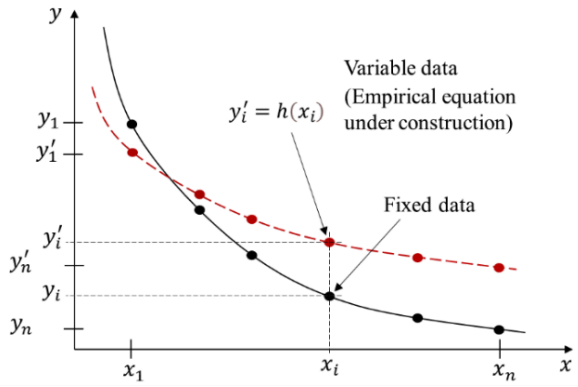

Figure 2. Fixed data and variable data positions

The empirical equation $y'_i = h(x_i)$ has coefficients a_i and exponents n_j, and for its calibration, computational tools are required, and one of them is the Excel *Solver*.

In the Excel *Solver*, the sum of the squared error Σe^2 is assigned as the objective function in order to minimize, and the coefficients and exponents of the em–pirical equation under construction are assigned as va–riable cells. The purpose is for y'_i to be as close as pos–sible to y'_i to reduce the squared error to the minimum so that the trajectory of the data of the empirical equa–tion is superimposed on the trajectory of the fixed data.

There are other tools, such as Lingo, R, Maple, Matlab, Fortran, and Python, among other similar, for which code must be structured to calculate the minimum of the objective function. On the other hand, for the Excel *Solver*, it is enough to enter the necessary data.

2.2 Data conditioning of the analytical equation

The analytical equation (3) was conditioned to generate the discrete Mach number data for two phases: the first phase was set for the Mach number range from 1 to 10, and the second phase for the Mach number range from 1 to 5 is expressed as $P_{oy}/P_{ox} = \left[M_x^2/\left(a+bM_x^2\right)\right]^n / \left[cM_x^2 - b\right]^m$. Being the expressions for the exponents $n = k/(k\text{-}1)$ and $m = 1/(k\text{-}1)$ and for the coefficients $a = 2/(k+1)$, $b = (k\text{-}1)/(k+1)$ and $c = 2k/(k+1)$. The nume–rical values of the coefficients and exponents for $k = 1.1$, $k = 1.2$, $k = 1.3$, $k = 1.4$, $k = 1.5$, $k = 1.6$ and $k = 1.67$ are presented in Table 1.

Discrete Mach number data was generated for 1.1, $k = 1.2$, $k = 1.3$, $k = 1.4$, $k = 1.5$, $k = 1.6$ and $k = 1.67$, in the range of $1 \leq M_x \leq 10$ and $297\text{x}10^{-9} < P_{oy}/P_{ox} \leq 1$; the Mach number is discretized with an increment $\Delta M_x = 0.01$ for the range of $1 \leq M_x \leq 2$ and $\Delta M_x = 0.1$ for $2 \leq$

$M_x \leq 10$. The discretization for $\Delta M_x = 0.01$ is in order to smooth the curve patch for values close to the position $P_{oy}/P_{ox} = 1$ and $M_x = 1$. In total, $n = 190$ was discretized for the range of $1 \leq M_x \leq 10$, used in the first phase, and $n = 170$ for $1 \leq M_x \leq 5$, used in the second phase.

Table 1. Values of coefficients and exponents of the equation (3)

k	n	m	a	b	c
1.1	11	10	0.95238	0.04761	1.04761
1.2	6	5	0.90909	0.09090	1.09090
1.3	4.33333	3.33333	0.86956	0.13043	1.13043
1.4	3.5	2.5	0.83333	0.16666	1.16666
1.5	3	2	0.80000	0.20000	1.20000
1.6	2.66666	1.66666	0.76923	0.23076	1.23076
1.67	2.49253	1.49253	0.74906	0.25093	1.25093

The discrete data generated by the analytical equation (3) were plotted for $1 \leq M_x \leq 10$, as shown in Fig. 3a in the initial position. And for a second graph, the position was reversed, becoming the data of the Mach number M_x of the abscissa to be the ordinate and the P_{oy}/P_{ox} data of the ordinate to be the abscissa, as shown in Fig.3b in the inverted position. The same figure shows that curve $k = 1.4$ is located in the center of the group of analytic curves, both in its initial and inverted position.

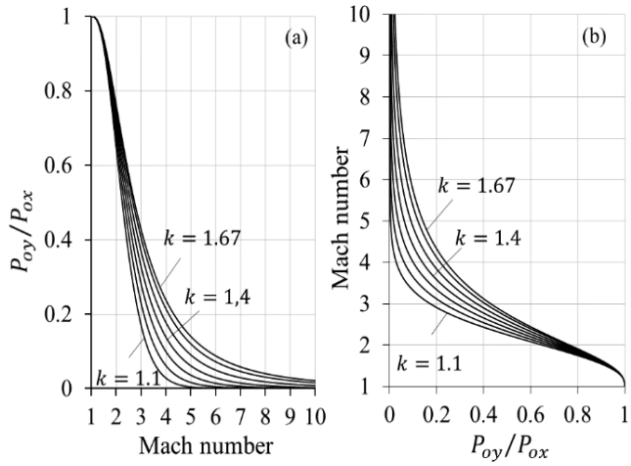

Figure 3. The behavior of the trajectories of the analytical curves. (a) Initial position. (b) Inverted position

The curves shown in Fig.3b are very important since the Mach number data of those curves are the fixed data, which belong to the exact solution of the analytical equation (3), and all the curves have a convergence point at position $M_x = 1$ and $P_{oy}/P_{ox} = 1$. And with the support of the standard data, the empirical equation will be constructed.

2.3 Coefficient of determination and percentage error

The coefficient of determination R^2 is calculated with equation (8) [29]:

$$\sum_{n=1}^{n}\left(Y-\bar{Y}\right)^2 = \sum_{n=1}^{n}\left(M_{x,a}-\sum M_{x,a}/n\right)^2 \quad (8)$$

The sum of the squared error is expressed as:

$$\sum_{n=1}^{n} e^2 = \sum_{n=1}^{n}\left(M_{x,a}-M_{x,e}\right)^2 \quad (9)$$

where n is the number of discrete Mach number data, the same quantity for the analytical and empirical equations, it should be noted that during the construction of the empirical equation, the sum of the squared error must be considered as the minimum of the objective function in the Excel *Solver*.

For calculation purposes, the Mach number of the analytical equation (3) is represented as $M_{x,a}$ which is fixed standard data, and of the empirical equation as $M_{x,e}$, which is variable data, which is based on the squared error conditioning principle $e^2 = (M_{x,a} - M_{x,e})^2$.

The variance of the dependent variable is expressed as:

$$\sum_{n=1}^{n}\left(Y-\bar{Y}\right)^2 \quad (10)$$

The average of discrete $M_{x,a}$ is expressed as $\bar{Y} = \sum M_{x,a}/n$. Each data of Y corresponds $Y = M_{x,a}$; therefore

$$\sum_{n=1}^{n}\left(Y-\bar{Y}\right)^2 = \sum_{n=1}^{n}\left(M_{x,a}-\sum M_{x,a}/n\right)^2$$

The following expression determines the percentage error e of the Mach number:

$$e = 100\left|\frac{M_{x,e}-M_{x,a}}{M_{x,a}}\right| \quad (11)$$

2.4 Solver iterative simulation analysis tool

Excel *Solver* version 2019 was used to calibrate the coefficients and exponents of the empirical equation. And its use was based on the fact that it is a versatile and easy-to-use tool to optimize the minimum of the sum of the squared error set as the objective function. In addition to including within the options the generalized reduced gradient method (GRG) [30] for nonlinear optimization solutions, it facilitates the search for solutions for the calibration of coefficients and expo–nents without restrictions during the construction of the empirical equations.

Table 2 presents the parameters and options in Excel*Solver* that are applied to calibrate the coefficients and exponents of the empirical equation.

Table 2. Parameters and options in the Solver tool

Parameter
Objective function cell: sum of square error
Objective cell condition: minimum
Changing variable cells: coefficients and exponents
Subject to restrictions: no restrictions
Option
Estimate: squared
Derivatives: central
Iterative method: GRG Nonlinear

Solver options considered it for time 10000 seconds and 10000 iterations. As *Solver* considers evaluating between zero and one, the range of accuracy and con–vergence, as well as tolerance equal to or greater than

zero; for these three options, the decimals were set to 10^{-12}. The closer to zero, the accuracy, tolerance, and convergence, the better the results; however, more time is required to get the minimum objective function's solution during optimization. It should be noted the decimal numbers that Excel takes into account in its spreadsheets are up to 10^{-15}.

2.5 Construction of the empirical equation

This section presents the steps of constructing the em–pirical equation for the Mach number range from 1 to 10.

As a strategy, as an initial phase, the empirical equation for the curve $k = 1.4$ is built since it is located in the center of the family of curves, later with the empirical equation obtained, it is approached for the other curves to calibrate their coefficients and exponents as discrete data; and as a final phase, the coefficients and exponents are calibrated as a function of k.

The steps to construct the empirical equation $M_x = f(P_{oy}/P_{ox})$ for the curve $k = 1.4$, are as follows:

Step 1: It was taken as a reference that the empirical curve begins at $P_{oy}/P_{ox} = 1$ and $M_x = 1$, the convergence point for all analytical and empirical curves. It is known that the ratio of stagnation pressures is in the range of $297\text{x}10^{-9} < P_{oy}/P_{ox} \leq 1$ on the abscissa axis and of Mach number in the range of $1 \leq M_x \leq 10$ on the ordinate axis.

Within the family of functions, the natural logarithm function $M_x = ln(P_{oy}/P_{ox})$ has the virtue of evaluating the argument for $P_{oy}/P_{ox} = 1$, where $M_x = ln(1) = 0$. Therefore, the beginning of the construction of the empirical equation is given by equation (12):

$$M_x = \ln\left(\frac{P_{oy}}{P_{ox}}\right) \tag{12}$$

The graph of the curves of the analytical and empirical equations is shown in Fig.4a. Where the empirical curve registers negative Mach number values and is out of phase, and starts at the position $P_{oy}/P_{ox} = 1$ and $M_x = 0$; therefore, equation (12) must be manipu–lated to adjust its behavior on the analytical curve.

Step 2: To translate the curve on the ordinate axis, the unit was added to equation (12); in addition, the argument P_{oy}/P_{ox} of the logarithm became the deno–minator to flip the curve, for which a new equation (13) was obtained. The graph of the empirical curve is shown in Fig.4b, where the Mach number has positive values, and the curve begins at the position $P_{oy}/P_{ox} = 1$ and $M_x = 1$:

$$M_x = 1 + \ln\left(\frac{1}{\frac{P_{oy}}{P_{ox}}}\right) \tag{13}$$

Step 3: This step adds coefficients and exponents to equation (13) to fit the curve. As coefficients and exponents are added in each step, the iteration is done in *Solver*, which is routinely repeated.

The logarithm was raised to the power p, as shown in the new equation (14). As an initial condition, $p = 1$ was established to start the iteration. By minimizing the sum of the squared error, which is the objective function, *Solver* gave $p = 1.253343$. The graph of the curves in Fig.4c shows that the empirical curve is closer to the analytical curve:

$$M_x = 1 + \left[\ln\left(\frac{1}{\frac{P_{oy}}{P_{ox}}}\right)\right]^p \tag{14}$$

Step 4: The above equation was raised to the power $n = 1$ and $p = 1.253343$ as shown in equation (15); *Solver* reported $n = 1.491785$ and $p = 0.712427$. In Fig. 4d, it is shown that the empirical curve is more in line with the analytical curve:

$$M_x = \left[1 + \left[\ln\left(\frac{1}{\frac{P_{oy}}{P_{ox}}}\right)\right]^p\right]^n \tag{15}$$

Step 5: The term $(P_{oy}/P_{ox})^m$ was added to divide the previous equation and the coefficient a to multiply; as shown in equation (16), $m = 0.1$ and $a = 1$ were assigned, and the values $n = 1.491785$ and $p = 0.712427$. When optimizing, *Solver* reported: $m = 0.150776$, $a = 0.947419$, $p = 0.389651$, $n = 1.349928$. In this step, the empirical curve was superimposed on the analytical curve, as shown in Fig. 4e:

$$M_x = \frac{\left[1 + a\left[\ln\left(\frac{1}{\frac{P_{oy}}{P_{ox}}}\right)\right]^p\right]^n}{\left(\frac{P_{oy}}{P_{ox}}\right)^m} \tag{16}$$

For equation (16), the percentage error reached a maximum peak $e < 0.9\%$ for the region of Mach number close to 1; for other regions, the error was below $e < 0.35\%$, as shown in Fig. 4f. In addition, the coefficient of determination $R^2 = 0.999996$ was obtained, close to $R^2 \approx 1$; and the sum of the squared error yielded $\Sigma e^2 = 0.075$.

It should be noted that Fig. 4 illustrates the evolution of the empirical curves on the inverse analytical equation (3) curve for stages 1, 2, 3, 3, 3, 4, and 5 performed.

The error peak close to 0.9% is high despite having $R^2 \approx 1$. Therefore, the empirical equation (16) must be adapted, and another term must be added to reduce the error.

This consideration of reducing the error allows better numerical precision; in this way, the results of the empirical equation will be more adjusted to the numerical data of the analytical equation (3). Therefore, a new empirical equation has to be obtained, which is presented in step 6.

Step 6: The new empirical equation (17) is presented in this step.

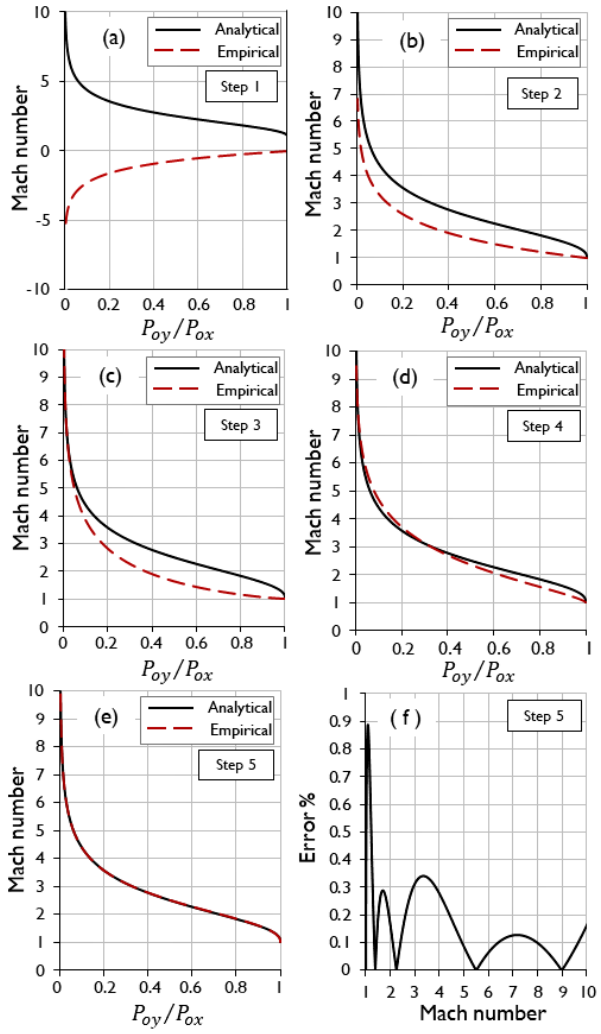

Figure 4. The behavior of the evolution and adjustment of the empirical curve on the analytical curve for k = 1.4. (a) Step 1, (b) step 2, (c) Step 3, (d) Step 4, (e) Step 5, and (f) Mach number percentage error for step 5.

$$M_x = \left[\frac{1}{\left(\frac{P_{oy}}{P_{ox}}\right)^{n_1}} + \frac{a_1 \left[\ln\left(\frac{1}{\frac{P_{oy}}{P_{ox}}}\right)^{n_3} \right]}{\left(\frac{P_{oy}}{P_{ox}}\right)^{n_2}} \right]^{n_4} + a_2 \left(\frac{P_{oy}}{P_{ox}}\right)^{n_5} \left[\frac{1}{\left(\frac{P_{oy}}{P_{ox}}\right)^{n_6}} - 1 \right]^{n_7} \quad (17)$$

The procedure to obtain equation (17) $M_x = f(P_{oy}/P_{ox})$ is as follows: the nomenclature of the coefficients was adapted as a_i and that of the exponents as n_j. Equation (16), the section of the first term, was taken as the basis. The second term was carefully constructed to satisfy the decrease of the error percentage and increase the exact decimal digits of the Mach number.

For a prior adjustment of the coefficients and exponents of equation (17), the *Solver* was not applied; therefore, the calibration was manual. To avoid divergence of the sum of the squared error, the assignment of the coefficient and exponent values was controlled so that the sum of the squared error was less than unity. A series of numerical tests were performed, and the most satisfactory results, which are four tests, are presented in Table 3. It should be noted that the values of a_1, n_1, n_2, n_3, and n_4 in tests 1 and 2 correspond to the data generated in step 5 for equation (16).

Table 3. Manually calibrated values of coefficients and exponents for k = 1.4

Test	1	2	3	4
		Coefficient		
a_1	0.947419	0.947419	0.5	0.5
a_2	1	0.5	1	1.2
		Exponent		
n_1	0.150776	0.150776	0.1	0.1
n_2	0.150776	0.150776	0.1	0.1
n_3	0.389651	0.389651	0.3	0.33
n_4	1.349928	1.349928	1.8	1.81
n_5	1	0.5	0.1	0.07
n_6	1	0.5	0.5	0.15
n_7	1	0.5	0.5	0.6
Σe^2	548.2	296.2	32.95	0.05
Error %	46	37	13	0.8

From Table 3, test 4 was the most satisfactory since it has the percentage error of Mach number less than 1%, and the sum of the squared error Σe^2 = 0.05. Therefore, the data from test 4 were taken as the initial condition to calibrate the coefficients and exponents with the *Solver*.

To optimize the minimum of the sum of the squared error, as an objective function, the following was taken into account changing variable cells: a1, a2, n_1, n_2, n_3, n_4, n_5, n_6 and n_7, and without restrictions. Consecutive repetitions of runs were performed until numerical convergence was obtained, the calibrated values of coefficients a_1 = 0.476086 and a_2 = 1.245852, and the exponents n_1 = 0.108771, n_2 = 0.091835, n_3 =0.328732, n_4 = 1.821138, n_5 + 0,083785, n_6 = 0.176509, and n_7 = 0.618819, respectively.

Fig. 5a illustrates the empirical curve superimposed on the analytical curve, and Fig. 5b shows the percentage error curve of the Mach number. The error reached the maximum peak e < 0.012% for the region of Mach number close to 1, the smallest error concerning equation (16) which has a peak of e < 0.9%. In addition, the coefficient of determination R^2 = 0.999996 was obtained, close to $R^2 \approx 1$, and the sum of the squared error yielded $\Sigma e^2 = 9.9864 \times 10^{-7}$.

With equation (17) already constructed in its final stage, the coefficients and exponents of the curves of the extremes were determined for for k = 1.1, k = 1.2, k = 1.3, k = 1.4, k = 1.5, k = 1.6 and k = 1.67. *For* example, to calibrate the a_i and n_j for k = 1.3, we took as initial data the a_i and n_j obtained for k = 1.4, applied the

Solver, and obtained the new values of a_i and n_j for k = 1.3. Similarly, we calibrated the a_i and n_j for the other k values. The values of the calibrated a_i and n_j for the Mach number range from 1 to 10 are presented in the resultsin Tables 4 and 5. Similarly, with equation (17), a_i and n_j were calibrated for the Mach number range from 1 to 5. The values are presented in the resultsin Tables 7 and 8.

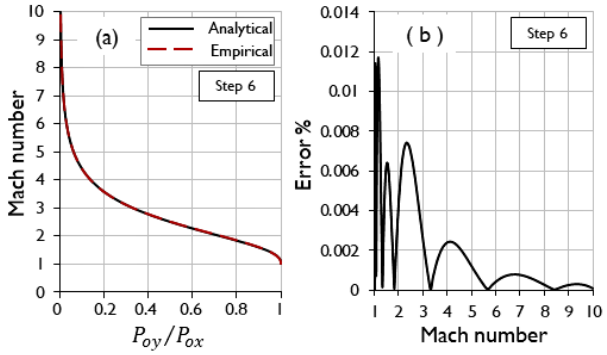

Figure 5. The behavior of the evolution and adjustment of the empirical curve on the analytical curve for k = 1.4 (a) Step 6, and (b) Mach number percentage error for step 6.

To obtain equation (17) $M_x = f(P_{oy}/P_{ox},k)$ as a function of two variables, with the discrete data of the coefficients and exponents for each value of k. For example, for each data of k = 1.1, k = 1.2, k = 1.3, k = 1.4, k = 1.5, k = 1.6 and k = 1.67 we have the values of the coefficients a_i and the exponent n_j, so that with these data we construct the polynomials $a_i = f(k)$ and $n_j = f(k)$, which are the initial data to apply the Solver.

The data in Tables 4 and 5 were used for the Mach number in the range 1 to 10, and Tables 7 and 8 were used for the Mach number in the range 1 to 5.

This phase of polynomial calibration started with the smoothest curve that reported the discrete data and was anchored as fixed and constant data. The remainder of the discrete data was taken as variables in the changing cell and re-optimized to obtain new values of coef–ficients and exponents. Then, the smoothest curve trajectory was searched again, anchored as a constant value, and optimized until new values of the remaining discrete data were recorded. The procedure was repeated until the last polynomial was obtained. It was very complicated beca–use it was trial and error. The poly–nomials obtained are shown in the results; the Mach number range from 1 to 1 is presented in Table 6, and for Mach number range from 1 to 5 is presented in Table 9.

3. RESULTS AND DISCUSSION

This section presents the results for four case studies, calculated with the empirical equation (17): two cases for $1 \le M_x \le 10$, one for a_i and n_j, and another for $a_i = f(k)$ and $n_j = f(k)$. And two cases for $1 \le M_x \le 5$, one for a_i and n_j, and another for $a_i = f(k)$ and $n_j = f(k)$.

3.1 Case studies

For case 1, in Tables 4 and 5, the results are presented; it was evaluated for discrete data, where the coefficients a_1 and a_2 and of the exponents n_1, n_2, n_3, n_4, n_5, n_6 and n_7 were calibrated for each value of k, for $M_x = f(P_{oy}/P_{ox})$ in the range of $1 \le M_x \le 10$. For case 2, Table 6 presents the results; it was evaluated for polynomials, where the coefficients $a_i = f(k)$, and of the exponents $n_j = f(k)$, for $M_x = f(P_{oy}/P_{ox},k)$ in the range of $1 \le M_x \le 10$.

Case 3 was evaluated similarly to case 1, considering the range of $1 \le M_x \le 5$; the results are pre–sented in Tables 7 and 8. Likewise, case 4 was evaluated similarly to case 2, for the range of $1 \le M_x \le 5$; the results are presented in Table 9.

Table 4. Case 1 (discrete).Values of coefficients and expo–nents for $1 \le M \le 10$

	Specific heats ratio, k			
	1.1	1.2	1.3	1.4
	Coefficient			
a_1	0.492179	0.479552	0.476537	0.476086
a_2	1.086264	1.178176	1.254848	1.245852
	Exponent			
n_1	0.026083	0.052875	0.081332	0.108771
n_2	0.017577	0.045007	0.069289	0.091835
n_3	0.331909	0.329867	0.328471	0.328732
n_4	1.827822	1.835295	1.817479	1.821138
n_5	0.062189	0.073795	0.075084	0.083785
n_6	0.169086	0.165590	0.166910	0.176509
n_7	0.684540	0.650321	0.628955	0.618819

Table 5. Case 1 (discrete).Values of coefficients and exponents for $1 \le M \le 10$ (continued)

	Specific heats ratio, k		
	1.5	1.6	1.67
	Coefficient		
a_1	0.459335	0.452209	0.448856
a_2	1.176689	1.112404	0.987731
	Exponent		
n_1	0.134325	0.158001	0.174837
n_2	0.110978	0.133166	0.150141
n_3	0.327411	0.326984	0.326356
n_4	1.862755	1.885781	1.891396
n_5	0.094015	0.106094	0.126569
n_6	0.208957	0.245299	0.319088
n_7	0.605354	0.598374	0.594572

Table 6. Case 2 (polynomial). Values of coefficients and exponents as a function of k, for $1 \le M \le 10$

Coefficient
$a_1 = 0.3142k^4 - 1.8391k^3 + 4.0145k^2 - 3.9103k + 1.919$
$a_2 = 70.796k^4 - 406.37k^3 + 865.67k^2 - 811.33k + 283.7$
Exponent
$n_1 = -0.0378k^4 + 0.2521k^3 - 0.5816k^2 + 0.8404k - 0.4757$
$n_2 = -0.0019k^2 + 0.2542k - 0.254$
$n_3 = -0.0126k^2 + 0.0282k + 0.3119$
$n_4 = -1.2384k^4 + 7.2241k^3 - 15.887k^2 + 15.527k - 3.881$
$n_5 = -2.9764k^4 + 17.769k^3 - 39.184k^2 + 37.918k - 13.543$
$n_6 = -8.2402k^4 + 49.594k^3 - 109.6k^2 + 105.8k - 37.583$
$n_7 = -0.1164k^3 + 0.6056k^2 - 1.1321k + 1.3324$

Table 7. Case 3 (discrete). Values of coefficients and exponents for $1 \le M \le 5$

	Specific heat ratio, k			
	1.1	1.2	1.3	1.4
	Coefficient			
a_1	0.537840	0.511532	0.496921	0.488949
a_2	1.176279	1.229231	1.251125	1.291484
	Exponent			
n_1	0.015236	0.014004	0.018284	0.020207
n_2	0.019383	0.058125	0.089087	0.119308
n_3	0.334694	0.334831	0.334934	0.335207
n_4	1.720268	1.816176	1.878027	1.922165

n_5	0.054244	0.063208	0.058474	0.046825
n_6	0.173349	0.197771	0.224437	0.250492
n_7	0.727952	0.735660	0.738437	0.744708

Table 8. Case 3 (discrete). Values of coefficients and exponents for 1 ≤ *M* ≤ 5 (continued)

	Specific heats ratio, k		
	1.5	1.6	1.67
	Coefficient		
a_1	0.479420	0.472944	0.467792
a_2	1.281022	1.304331	1.310532
	Exponent		
n_1	0.022130	0.027203	0.034554
n_2	0.147488	0.177197	0.198434
n_3	0.335485	0.335462	0.335182
n_4	1.975362	2.012170	2.035745
n_5	0.036499	0.022511	0.013486
n_6	0.288247	0.311133	0.323000
n_7	0.750570	0.749942	0.744086

Table 9. Case 4 (polynomial). Values of coefficients and exponents as a function of *k*, for 1 ≤ *M* ≤ 5

Coefficients
$a_1 = 0.034k^3 - 0.116k^2 + 0.1286k + 0.4851$
$a_2 = 0.0228k^3 - 0.1375k^2 + 0.2828k + 0.9883$
Exponents
$n_1 = 0.1878k^4 - 0.9798k^3 + 1.8897k^2 - 1.5298k + 0.4473$
$n_2 = 0.0526k^3 - 0.2254k^2 + 0.6634k - 0.502261$
$n_3 = 0.333333$
$n_4 = -0.221k^4 + 1.0635k^3 - 1.8905k^2 + 1.5326k + 1.22594$
$n_5 = 0.3377k^3 - 1.5728k^2 + 2.341k - 1.0537$
$n_6 = -0.086k^3 + 0.3613k^2 - 0.1311k - 0.0116$
$n_7 = -0.0385k^3 + 0.1431k^2 - 0.1518k + 0.7475$

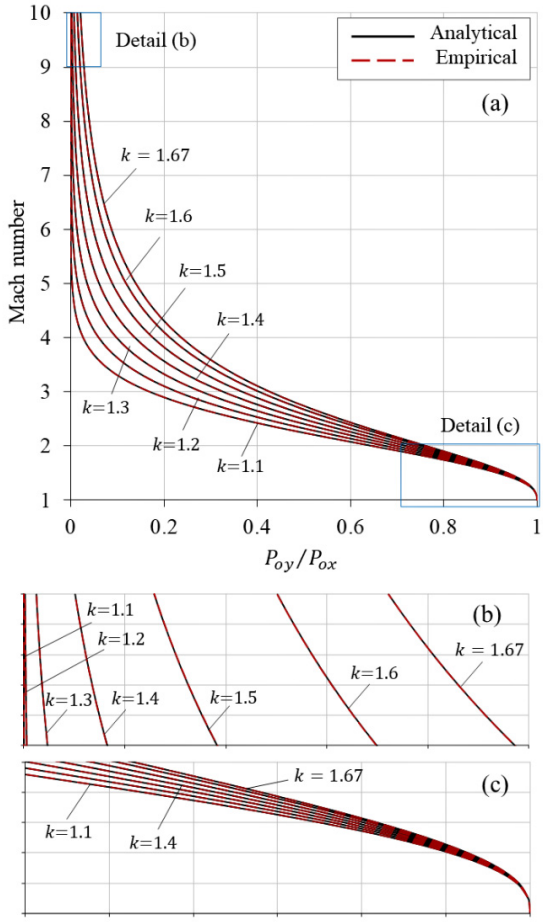

Figure 6. Case 2. (a) Empirical curves superimposed on the analytical curves. (b) and (c) Detail.

The empirical curves obtained with equation (17) and data from Table 6 of case 2, for $M_x = f(P_{oy}/P_{ox},k)$ in the range of $1 \le M_x \le 10$, are shown in Fig.6a. An enlarged detail of the ends of the family of curves is shown in Fig. 6b and Fig. 6c. It is observed that all the empirical curves (equation (17)) are superimposed on the analytical curves (equation (3)) for k = 1.1, k = 1.2, k = 1.3, k = 1.4, k = 1.5, k = 1.6 and k = 1.67 respectively.

All the analytical and empirical curves converge at the position P_{oy}/P_{ox} = 1 and M_x = 1. It should be noted that the graphs of case 2. Cases 1, 3, and 4 are not included since the trajectories of the curves are similar. In addition, it is indicated that cases 3 and 4 only cover the range of $1 \le M_x \le 5$.

3.2 Comparative analysis of cases

The Mach number values obtained with the empirical equation (17) are compared with the exact values of the analytical equation (3). They are only considered for k = 1.1, k = 1.3 k = 1.5 and k = 1.67; the other values of for k = 1.2, k = 1.4, k = 1.6, the results are similar.

In Tables 10,11, 12, and 13, the proximity to the exact solution is evidenced when comparing the results of the empirical equation. How the decimals fluctuate by excess and by default indicates that the empirical curves oscillate and intercept with analytical curves. For case 1 (Table 10), the Mach number error is less than 0.018%; for case 2 (Table 11), the error is less than 0.063%; for case 3 (Table 12), the error is less than 0.004%, finally, for case 4 (Table 13) the error is less than 0.00988%.

Table 10. Case 1 (discrete). Mach number values calculated with the empirical equation (17) and Tables 4 and 5

	Specific heats ratio, k			
	1.1	1.3	1.5	1.67
	Mach number			
Analytical	Empirical			
1	1.000000	1.000000	1.000000	1.000000
2	2.000014	1.999944	1.999909	1.999920
3	2.999841	2.999897	2.999975	3.000035
4	4.000064	4.000074	4.000086	4.000066
5	5.000097	5.000063	5.000029	4.999984
6	5.999964	5.999982	5.999963	5.999947
7	6.999913	6.999948	6.999959	6.999980
8	8.000008	7.999977	7.999998	8.000034
9	9.000083	9.000021	9.000025	9.000035
10	9.999912	9.999975	9.999979	9.999905

Table 11.Case 2 (polynomial). Mach number values calcu–lated with the empirical equation (17) and Table 6

	Specific heats ratio, k			
	1.1	1.3	1.5	1.67
	Mach number			
Analytical	Empirical			
1	1.000000	1.000000	1.000000	1.000000
2	2.000692	2.000283	2.000669	1.999579
3	3.000916	3.000661	3.001670	2.999569
4	4.001232	4.001270	4.002457	3.999529
5	5.001418	5.001636	5.002705	4.999276
6	6.001357	6.001882	6.002638	5.998966
7	7.001175	7.002167	7.002464	6.998694
8	8.000942	8.002634	8.002294	7.998488
9	9.000591	9.003237	9.002179	8.998384
10	9.999845	10.00000	9.999974	9.999915

The most accurate values are for discrete data; however, they have the disadvantage that they are individual curves for each k value.

While the empirical equation with the data of coefficients and exponents as a function of k allows dealing with a family of curves within the range of $1.1 \leq k \leq 1.67$, the advantage is much greater regarding individual curves.

Table 12. Case 3 (discrete). Mach number values calculated with the empirical equation (17) and Tables7 and 8

	Specific heats ratio, k			
	1.1	1.3	1.5	1.67
	Mach number			
Analytical	Empirical			
1	1.000000	1.000000	1.000000	1.000000
2	2.000002	1.999996	1.999996	1.999985
3	2.999995	3.000003	3.000004	3.000014
4	4.000005	3.999999	3.999999	3.999993
5	5.000056	5.000050	5.000050	5.000073

Table 13. Case 4 (polynomial). Mach number values calculated with the empirical equation (17) and Table 9

	Specific heats ratio, k			
	1.1	1.3	1.5	1.67
	Mach number			
Analytical	Empirical			
1	1.000000	1.000000	1.000000	1.000000
2	1.999972	1.999991	2.000016	2.000052
3	3.000160	3.000204	3.000208	3.000290
4	4.000368	4.000251	4.000082	4.000060
5	5.000486	5.000164	4.999690	4.999507

The results of the Mach numbers presented in Tables 10-13 have to do with the calibrations of the coefficients and exponents. The solution search engine by iterative methods in *Solver* was based on the GRG. The unrestricted condition was applied to the variables, where the objective function was the minimum sum of the squared error.

The calibration phase to obtain the polynomials $a_i = f(k)$ and $n_j = f(k)$ presented difficulty and was very laborious because the discrete data for each value of k did not only present curves but also fluctuations. In addition, this was compounded by the fact that the errors during calibration increased rather than remained the same or decreased. Therefore, to avoid sharp increases in the errors, the polynomials of orders 2, 3, and 4 were evaluated repeatedly, and the one with the lowest error was selected, and this was done for each coefficient and exponent. It should be noted that sometimes the errors increased above 2%, which is why we tried to obtain the errors as close as possible to the discrete data values.

It is summarized, in Table 14 shows the magnitudes of the percentage errors of the Mach number and the coefficients of determination $R^2 \approx 1$ for the four cases of study. Figure 7 shows the behavior of the Mach number errors for the four cases.

Table 14. Comparative table of cases for different ranges of Mach number

Cases	Mach number	Error %	Coefficient of determination
1 (discrete)	1-10	0.018	0.99999
2 (polynomial)	1-10	0.063	0.99999
3 (discrete)	1-5	0.004	0.99999
4 (polynomial)	1-5	0.00988	0.99999

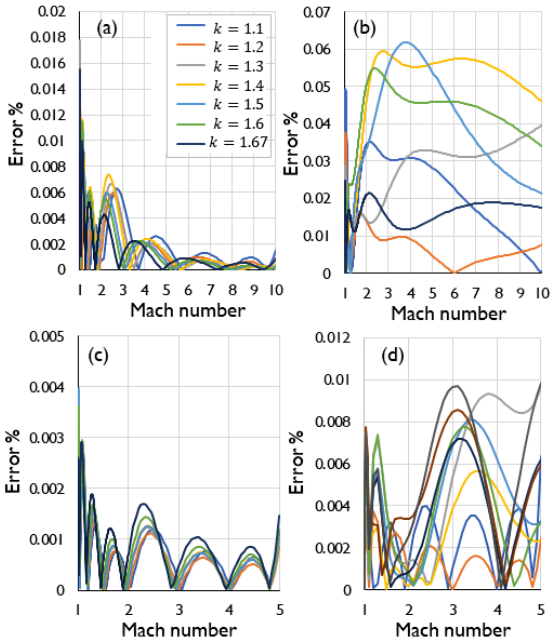

Figure7. Percentage errors of Mach number. (a) Case 1, (b) Case 2, (c) Case 3, and (d) Case 4

The empirical equation (17) is a mathematical representation of the solution of the inverse of equation (3). It significantly contributes to the area of gas dynamics for quasi-one-dimensional isentropic compressible flow. However, it can be improved by modifying or adding more terms to reduce the error further.

The analytical equations (3) and (4), among other mathematical expressions, are widely used to simulate the compressible flow in one dimension for an ideal gas or real gas, for which different computational iterative calculation procedures are applied to obtain the solutions [31-36].

Applying the empirical equation (17), the following are considered for the design of a nozzle at Mach 3, flow $k = 1.4$ and $A_x/A^* = 4.234$. The inlet pressure of the nozzle $P_0 = 3.5547$ atm is considered a constant value, and the pressure at outlet Pe is variable. For the divergent shock to occur,the pressure ratio $rp = P_e/P_0$ is $0.2183 < rp < 0.9866$, and the Mach number at the outlet is $0.1384 < M_e < 0.4751$. For the shock to occur in the divergent section, the outlet pressure P_e is $1 < P_e < 3.5075$; for this range, four cases are established: $rp = 0.4$; $rp = 0.5$; $rp = 0.6$ and $rp = 0.7$.

The behavior patterns of the trajectories of the curves for the Mach number and how the normal shocks are distributed in the local positions in A_x/A^* for the supersonic flow M_x and subsonic flow M_y are shown in Fig. 8. As the magnitude of rp decreases, the position of the shock is translated toward the nozzle outlet.

It should be noted that the curve span for the supersonic flow up to the shock position and for the subsonic flow after the shock is determined with equation (4) for each position of A/A^*. The subsonic Mach number, after the shock, from M_y to M_e, is calculated with the area ratio $A/A_y^* = \left(A/A_x^*\right) / \left(A_y^*/A_x^*\right)$. For A/A_x^*, the area A_x^* is the critical area in the throat, the value of A is variable in the range from

A_y to A_e, and the ratio A_y^*/A_x^* is a constant value. When a shock wave is present, the critical area A^* increases as the wave passes through; therefore, the ratio of critical areas, before the shock A_x^* and after the shock A_y^*, is determined by equation (18):

$$\frac{A_y^*}{A_x^*}=\frac{M_y}{M_x}\left[\frac{2+(k-1)M_x^2}{2+(k-1)M_y^2}\right]^{\left(\frac{k+1}{2k-2}\right)} \tag{18}$$

The empirical equation (17) facilitated the calculations by connecting with the analytical equations involved (1), (2), (4), (5), (6), and (18) to obtain the curves shown in Fig. 8.

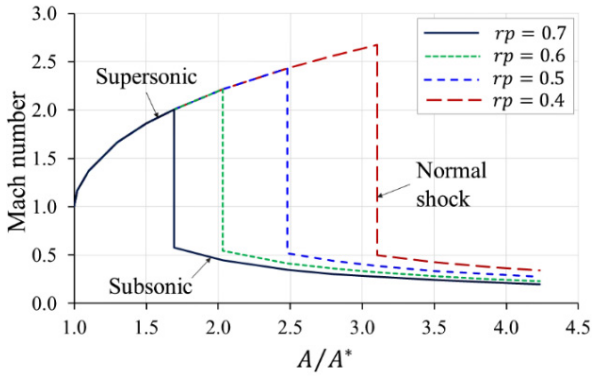

Figure8. Mach number patterns in the divergent for flow with *k* = 1.4

Table 15 presents the magnitudes of the parameters at the shock position A_x/A^*, for rp = 0.4, rp = 0.5, rp = 0.6 and rp = 0.7.

Table 15. Magnitudes of the parameters in the position of the shock corresponding to Fig.8

Parameter	Pressure ratio, rp			
	0.4	0.5	0.6	0.7
P_{oy}/P_{ox}	0.432	0.526	0.621	0.718
M_x	2.674	2.433	2.213	2.004
M_y	0.497	0.519	0.545	0.576
P_y/P_x	8.175	6.740	5.551	4.521
A_x/A^*	3.105	2.478	2.029	1.694

In convergent-divergent nozzles for the over-expanded flow condition, and according to the designs of the aerodynamic profiles of the walls, the shock wave can reach values close to Mach 5. Therefore, the empirical equation (17) and the data from Tables 7, 8, and 9, for the range of $1 \le Mx \le 5$ and $1.1 \le k \le 1.67$, is an appropriate and relevant option to be applied.

One of the control parameters is the percentage error to calibrate coefficients and exponents of empirical equations, which indicates how much the empirical curves should be adjusted to the analytical ones, and calibration is a laborious task.

4. CONCLUSIONS

The method applied to construct the empirical equation (17) shows that it is possible to obtain approximate solutions to certain problems of analytical equations that algebraic procedures cannot invert.

The empirical equation (17) is a mathematical representation that satisfies the solution of the inverse of the analytical equation (3). Therefore, it is a significant contribution to gas dynamics for a quasi-one-dimensional isentropic compressible flow.

The determination coefficients present values of R2≈1 for the four study cases. The coefficients and exponents of the empirical equation (17) for $\boldsymbol{1 \le M \le 10}$, the error is less than 0.018% for the discrete data and less than 0.063% for the polynomials. Likewise, $\boldsymbol{1 \le M_x \le 5}$ presents the Mach number error of less than 0.004% for the discrete data and less than 0.00988% for the polynomials.

REFERENCES

[1] Rotty, R.M.: Introduction to gas dynamics, Wiley, 1962

[2] Anderson, J.D.: Fundamentals of aerodynamics, McGraw-Hill Series in aeronautical and aerospace engineering, 2017.

[3] Sutton, G.P., Biblarz, O.: Rocket propulsion elements, John Wiley & Sons, 2017.

[4] Schlichting, H., Gersten, k.: Boundary-layer theory, Springer-Verlag Berlin Heidelberg, 2017.

[5] Mahapatra, S., Nelaturi, A., Tennyson, J.A., Ghosh, S.: Large-eddy simulation of compressible turbulent flow in convergent-divergent nozzles with isothermal wall, International Journal of Heat and Fluid Flow, Vol. 78, pp. 1-20, 2019. https://doi.org/10.1016/j.ijheatfluidflow.2019.108425

[6] Martelli, E., Saccoccio, L., Ciottoli, P., Tinney, C., Baars, W., Bernardini, M.: Flow dynamics and wall-pressure signatures in a high-Reynolds-number overexpanded nozzle with free shock separation, Journal of Fluid Mechanics, 895. A29. pp. 1-30, 2020. https://doi.org/10.1017/jfm.2020.280

[7] Génin, C., Stark, R., Karl, S.:Shock system deformation in high Mach number rocket nozzles, 31st International Symposium on Shock Waves 2, pp. 543–549, 2019. https://doi.org/10.1007/978-3-319-91017-8_69

[8] Zmijanović, V., Rašuo, B., Chpoun, A.: Flow separation modes and side phenomena in an over-expanded nozzle, FME Transactions, Vol. 40, No. 3, pp. 111-118, 2012.

[9] Östlun, J.: Flow processes in rocket engine nozzles with focus on flow separation and side-loads, Licentiate Thesis, Stockholm, 2002.

[10] Hagemann, G., Frey, M. and Koschel W.: Appearance of restricted shock separation in rocket nozzles, AIAA J. of Propulsion and Power, Vol. 18, No. 3, pp. 577-584, 2002.

[11] Hunter, C.: Experimental, theoretical, and computational investigation of separated nozzle flows, American Institute of Aeronautics and

Astronautics, 1998. https://doi.org/10.2514/6.1998-3107

[12] Tolentino, S.L.: Evaluation of turbulence models for the air flow in a planar nozzle, INGENIUS, No. 22, pp. 25–37, 2019. https://doi.org/10.17163/ings.n22.2019.03

[13] Sajben, M., Bogar, T.J., Kroutil J.C.: Forced oscillation experiments in supercritical diffuser flows with application to ramjet instabilities. AIAA/SAE/ASME, 17th Join Propulsion Conference, July 27-29, Colorado, 1981.

[14] Tolentino, S.L.: Evaluation of turbulence models for the air flow in a transonic diffuser, Polytechnic Journal, Vol. 45, No. 1, pp. 25-38, 2020. (In Spanish)

[15] Milićev, S.S.: An Experimental study of the influence of spike in supersonic and transonic flows past a hemispheric body, FME Transactions, Vol. 50, No. 1, pp. 24-31, 2022.https://doi.org/105937/fme2201024M

[16] Damljanović, D. and Rašuo, B.: Testing of calibration models in order to certify the overall reliability of the trisonicblowdown wind tunnel of VTI, FME Transactions, Vol. 38, No. 4, pp. 167-172, 2010.

[17] Damljanović, D., Vuković, D., Ocokoljić, G., Rašuo, B.: Convergence of transonic wind tunnel test results of the AGARD-B standard model, FME Transactions, Vol. 48, No. 4, pp. 761-769, 2020. https://doi.org/10.5937/fme2004761D

[18] Zarea, S., Irausquin, I., Leañez, E.: Experimental evaluation of eight SZ-1500 series airfoils for low Reynolds number, Journal of the Faculty of Engineering of UCV, Vol. 18, No. 3, pp. 157-177, 2003. (In Spanish)

[19] White, F.: Fluid Mechanics, USA: McGraw-Hill Education, 2016.

[20] Cengel, Y., Cimbala, J.: Fluid mechanics: Fundamentals and applications, McGraw-Hill, 2019.

[21] Polya, G.:How to solve it, Princeton Science Library Edition, 2004.

[22] Whittaker, E.T., Watson, G.N.: A Course of modern analysis, 4th ed. Cambridge University Press. Cambridge, 1927.

[23] Abu-Irshaid, E.M.:Asymptotic solutions for the fundamental isentropic relations in variable area duct flow, Master´s thesis, University of Tennessee, Knoxville, 2006.

[24] Majdalani, J., Maicke, B.:Explicit inversion of Stodola`s area-Mach number equation, Journal of Heat Transfer, Vol. 133, No. 7, pp.1-7, 2011.https://doi.org/10.1115/1.4002596

[25] Majdalani, J., Maicke, B.: Inversion of the fundamental thermodynamic equations for isentropic nozzle flow analysis, Journal of Engineering for Gas Turbines and Power, vol. 134, No. 3, pp.1-9, 2012. doi: 10.1115/1.4003963

[26] Ferrari, A.: Exact solutions for quasi-one-dimensional compressible viscous flows in conical nozzles, Journal of Fluid Mechanics, Vol.915, pp.1-21, 2021. https://doi.org/10.1017/jfm.2020.1158

[27] Mikata, Y., Walczak, W.S.: Exact analytical solutions of the Colebrook-White equation, Journal of Hydraulic Engineering, Vol. 142, No. 2, pp. 04015050 1-6, 2016. doi: 10.1061/(asce)hy.1943-7900.0001074

[28] Praks, P., Brkić, D.: Suitability for coding of the Colebrook's flow friction relation expressed by symbolic regression approximations of the Wright-ω function, Reports in Mechanical Engineering, Vol. 1, No. 1, pp. 174-179, 2020. https://doi.org/10.31181/rme200101174p

[29] Navidi, W.: Statistics for engineers and scientists, McGraw-Hill Companies, 2006.

[30] Lasdon, L.S. Fox, R.L. Ratner, M.W.: Nonlinear optimization using the generalized reduced gradient method, Recherche Opérationnelle, Tome 8, No. V3, pp. 73-103, 1974.

[31] Wornom, S.F., Hafez, M.M.: Calculation of quasi-one-dimensional flows with shocks. Computers & Fluids, Vol. 14, No. 2, pp. 131–140, 1986. https://doi.org/10.1016/0045-7930(86)90005-8

[32] Yang, J.,Martin, J.K.: Approximate solution—one-dimensional energy equation for transient, compressible, low Mach number turbulent boundary layer flows, Journal of Heat Transfer, Vol. 111, No. 3, pp. 619-624, 1989. https://doi.org/10.1115/1.3250727

[33] Sarimurat, M.N., Dang. T.: Shock management in diverging flow passages by blowing/suction. Part 1: Quasi-one-dimensional theory, Journal of Propulsion and Power, Vol. 28, pp. 1222-1229, 2012. https://doi.org/10.2514/1.B34136

[34] Maicke, B., Bondarev, B.: Quasi-one-dimensional modeling of pressure effects in supersonic nozzles, Aerospace Science and Technology, Vol.70, 161-169 2017. https://doi.org/10.1016/J.AST.2017.08.001

[35] Sirignano, W.A.: Compressible flow at high pressure with linear equation of state, Journal of Fluid Mechanics, Vol. 843, pp. 244-292, 2018.https://doi.org/10.1017/jfm.2018.166

[36] Gaitan, F.: Finding flows of a Navier-Stokes fluid through quantum computing, Quantum information, Vol.6, pp.1-6, 2020. https://doi.org/10.1038/ s41534-020-00291-0

NOMENCLATURE

a_i	Empirical equation coefficients
A_e	Area at the nozzle outlet
A_x	Area at shock position
A^*	Critical throat area
α	Half angle of divergent
β	Half angle of the convergent
e	Mach number percentage error
e^2	Squared error
GRG	Generalized reduced gradient

k	Specific heat ratio
M	Mach number
M_e	Mach number for subsonic flow, at the nozzle outlet
M_x	Mach number for supersonic flow at shock wave position
$M_{x,a}$	Mach number for discrete data from the analytical equation
$M_{x,e}$	Mach number for discrete data from the empirical equation
M_y	Mach number for subsonic flow at the position of the shock wave
n_j	Exponents of the empirical equation
P_e	Static pressure at the nozzle outlet
P_x	Static pressure at shock position for supersonic flow
P_o	Stagnation pressure at the nozzle inlet
P_{ox}	Stagnation pressure before the shock
P_y	Static pressure at shock position for subsonic flow
P_{oy}	Stagnation pressure after the shock
R^2	Coefficient of determination
r	Nozzle radius
rp	Pressure ratio
x	Reference point at the shock position for supersonic flow
y	Reference point at the shock position for subsonic flow

ЕМПИРИЈСКА ЈЕДНАЧИНА МАХОВОГ БРОЈА КАО ФУНКЦИЈА ОДНОСА СТАГНАЦИОНОГ ПРИТИСКА ЗА КВАЗИЈЕДНОДИМЕНЗИОНАЛНИ СТИШЉИВИ ПРОТОК

С.Л. Толентино

У овом раду за квази-једнодимензионални изентропски компресибилни модел струјања, конструисана је емпиријска једначина Маховог броја као функција односа притиска стагнације за аналитичку једначину коју алгебарске процедуре не могу да инвертују. Алат Екцел 2019 Солвер је примењен за калибрацију коефицијената и експонената емпиријске једначине током њене конструкције за опсег Маховог броја од 1 до 10 и 1 до 5. Специфични однос топлоте од 1,1 до 1,67 и генерализовани итеративни метод смањеног градијента су користи се за минимизирање суме квадратне грешке, која је постављена као циљна функција. Резултати показују да се за 1 до 10 маха добија грешка мања од 0,063%, а за 1 до 5 маха мања од 0,00988%. Закључује се да је добијена емпиријска једначина математички модел који репродукује путање обрнутих кривих проучаване аналитичке једначине.